

Investigation of vacuum polarization in t-channel radiative Bhabha scattering

D. Karlen ^a, H. Burkhardt ^b,

^a*Ottawa Carleton Institute for Physics, Carleton University, Ottawa, Canada K1S 5B6*

^b*CERN, SL Division, CH-1211 Geneva 23, Switzerland*

Abstract

We discuss the possibility of a precision measurement of vacuum polarization in t-channel radiative Bhabha scattering at a high luminosity collider. For illustration, the achievable precision is estimated for the BaBar experiment at PEP-II and for the OPAL experiment at LEP.

1 Introduction

There is a considerable interest in precision studies of electroweak physics. High energy data from LEP, SLC and Tevatron probe the electroweak theory on the quantum level. The radiative corrections are sensitive to the Higgs mass and provide constraints to theories beyond the standard model [1]. Very high precision measurements of the anomalous magnetic moment currently performed at Brookhaven [2] provide another very sensitive test of the standard model and beyond [3,4].

A major contribution to the radiative corrections is provided by the running of the electromagnetic coupling constant α from its value at vanishing momentum to the effective Q^2 of the process studied. The running of α can be expressed as

$$\alpha(Q^2) = \frac{\alpha(0)}{1 - \Delta\alpha_l(Q^2) - \Delta\alpha_{\text{had}}(Q^2)} \quad . \quad (1)$$

Email addresses: karlen@physics.carleton.ca (D. Karlen),
Helmut.Burkhardt@cern.ch (H. Burkhardt).

URLs: <http://www.physics.carleton.ca/~karlen> (D. Karlen),
<http://home.cern.ch/hbu/aqed/aqed.html> (H. Burkhardt).

Table 1

$\Delta\alpha_{\text{had}}$ and $\Delta\alpha_l$ at several energies in the t and s channel.

$\sqrt{s}, \sqrt{-t}$ GeV	$\Delta\alpha_{\text{had}}(t)$ %	$\Delta\alpha_{\text{had}}(s)$ %	$\Delta\alpha_l(s, t)$ %
0.1	0.009 ± 0.001	-0.009 ± 0.001	0.673
1	0.369 ± 0.009	-0.638 ± 0.054	1.253
1.5	0.524 ± 0.014	0.402 ± 0.015	1.375
10	1.463 ± 0.033	0.984 ± 0.048	2.099
91.188	2.758 ± 0.036	2.761 ± 0.036	3.142

The leptonic contribution $\Delta\alpha_l(s)$ can be calculated with high accuracy [5]. Theoretical predictions of the hadronic vacuum polarization have to rely on less well known concepts like non-perturbative QCD and light quark masses, or on experimental uncertainties in the evaluation of the dispersion integral (the P stands for the principal value)

$$\Delta\alpha_{\text{had}}(Q^2) = -\frac{\alpha Q^2}{3\pi} P \int_{4m_\pi^2}^{\infty} \frac{R_{\text{had}}(s')}{s'(s' - Q^2)} ds' \quad . \quad (2)$$

R_{had} is the measured QED cross-section of the process $e^+e^- \rightarrow \text{hadrons}$, normalized to the QED cross-section for lepton-pair production. Eq. (2) applies both to timelike or s-channel reactions with positive momentum squared ($Q^2 = s > 0$), as well as to spacelike or t-channel processes with negative momentum squared ($Q^2 = t < 0$). In the timelike, the integration has a singularity at $s = s'$. This gives a substantial weight to variations in the cross section close to the actual momentum squared of the process. $\Delta\alpha_{\text{had}}(s)$ can even become negative for energies where $R_{\text{had}}(s)$ is steeply increasing. Far from thresholds and resonances, one has $\Delta\alpha_{\text{had}}(Q^2) \approx \Delta\alpha_{\text{had}}(-Q^2)$.

For the details of the actual evaluation of the dispersion integral, we refer to the recently updated work by B. Pietrzyk and one of us [6]. Figure 1 and Table 1 list numerical values of $\Delta\alpha$ at several values of \sqrt{s} and $\sqrt{-t}$. The last column gives the leptonic contribution to first order, valid both for the s and t-channel (higher order corrections are known but actually smaller than the uncertainty in the hadronic contribution). Note that the hadronic vacuum polarization is known to about 2% at $t \approx -1 \text{ GeV}^2$. This corresponds to relative uncertainties of 0.6% in $\Delta\alpha$ and 0.9×10^{-4} in $\alpha(1 \text{ GeV}^2)$.

In this paper, we discuss the feasibility of a direct and precise measurement of the running of α in a single experiment, using radiative Bhabha scattering.

There are already a number of published papers with rather direct measurements of the energy dependence in vacuum polarization. Evidence for an observation of the

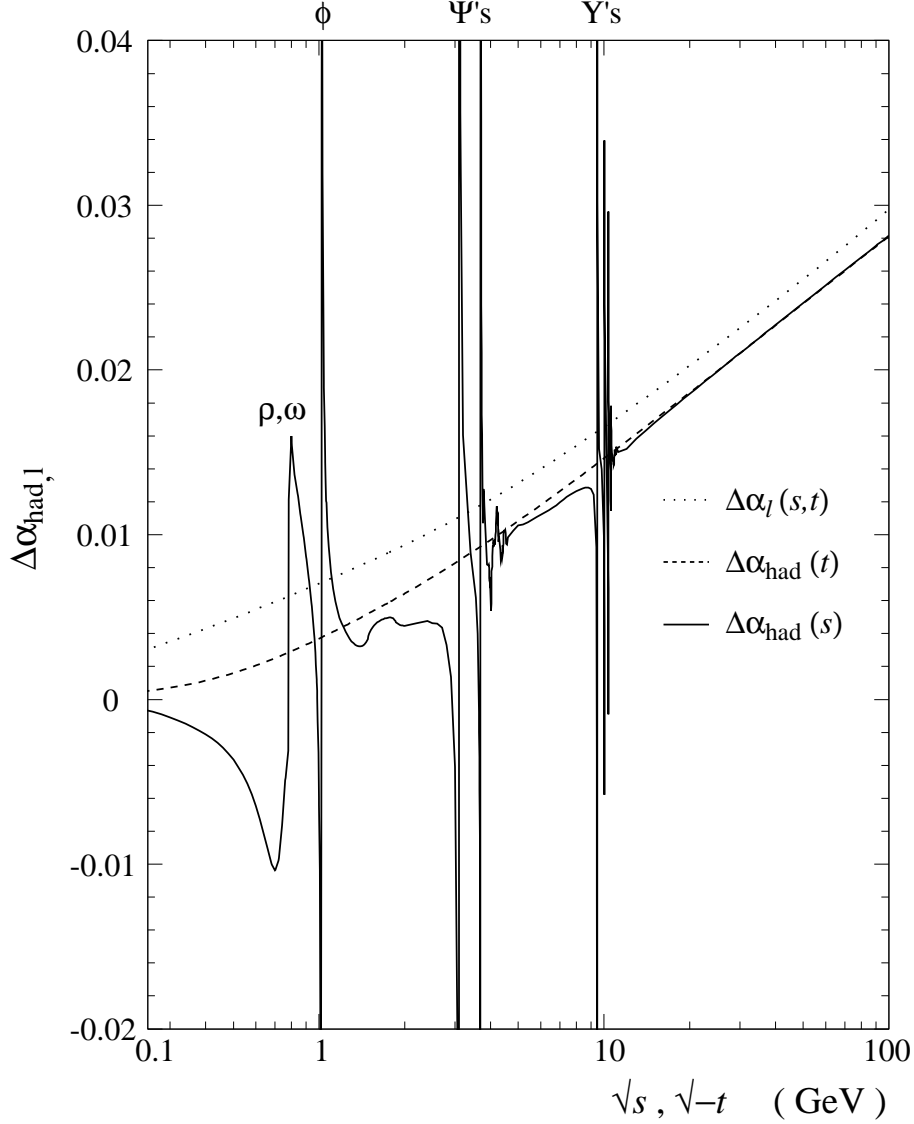


Fig. 1. $\Delta\alpha_l$ (dotted line) and $\Delta\alpha_{\text{had}}$ at several energies in the t (dashed line) and s channel (solid line).

hadronic vacuum polarization in the s -channel around the ϕ resonance for example was already reported in 1972 [7]. More recently, there have been measurements of α at $\sqrt{s} = 58$ GeV using muon-pair production [8,9]. Precise measurements of the angular distribution of Bhabha scattering have been interpreted as further evidence for the running of α in the range of $\sqrt{-t}$ from 10 to 54 GeV [9], and in the ranges 1.5 – 2.5 GeV and 3.5 – 58 GeV [10].

The potential advantage of a measurement based on radiative Bhabha scattering, as proposed in this paper, is the large cross-section of this process, and the possibility to cover a large range in Q^2 from some GeV down to essentially 0, in a single experiment.

2 t-channel radiative Bhabha scattering

The process shown in Fig. 2, when the exchanged photon is nearly real, can lead to a distinctive signature in e^+e^- collisions, that of a high energy coplanar photon and electron scattered at wide angles with the other electron scattered at a small angle [11–13]. In this note, the process will be referred to as TCRB scattering. The virtuality, Q^2 , of the exchanged photon is related to the scattering angle of the electron on the lower leg. A pole exists in the cross section for nearly zero degree scattering angles.

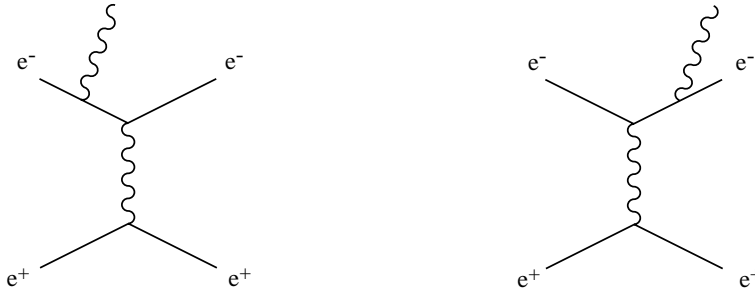


Fig. 2. The process of t-channel radiative Bhabha (TRCB) scattering in lowest order.

The event signatures are sketched in Fig. 3 for the two configurations that are used to measure vacuum polarization. For events in which the small angle scattered electron goes undetected, the dominant process has Q^2 nearly zero. When the small angle scattered electron is observed, the Q^2 of the exchanged photon depends on the scattering angle. The method we are proposing uses the ratio of the number of events in these two configurations to deduce the running of α .

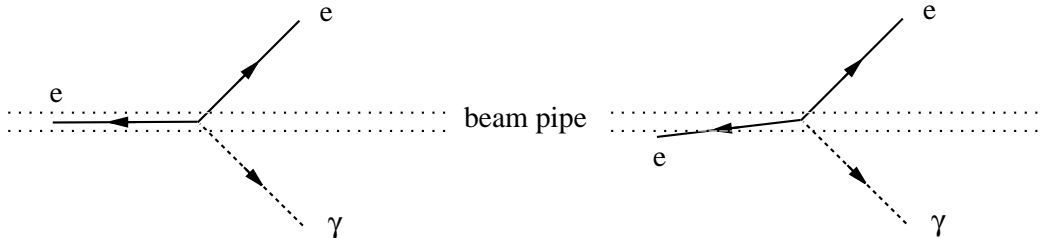


Fig. 3. Sketch of the kinematics. On the left, the case of very low Q^2 and on the right the process with higher Q^2 where all particles are detected.

3 Measurement of TCRB scattering at PEP-II

As an example, a measurement of TCRB scattering with the BaBar experiment at PEP-II with 500 fb^{-1} is considered. Collisions take place with a center-of-mass energy of 10.58 GeV and the center of mass is boosted with $\beta = 0.49$ in the direction of the electron (the positive z direction). Cross sections are calculated for an

Table 2

Summary of calculations for TCRB scattering for the BaBar acceptances. The first row shows the lowest order cross sections including the s and t channel contributions, but without vacuum polarization. The next row shows the number of events that would be collected (in millions) assuming an integrated luminosity of 500 fb^{-1} . The average Q^2 of the events in each bin is shown to vary from near 0 up to about 1.5 GeV^2 . The following row indicates the relative importance of the t channel contribution, compared to the cross section including all s and t diagrams. The corrections to α due to leptonic and hadronic loops are calculated using the repi program [6]. The average correction values are shown. The next line indicates the fractional change in cross sections that arise when the effects of vacuum polarization are included. The last line indicates the relative statistical precision of the event counts in each bin, which is small compared to the changes in the relative cross sections in the previous row.

	Range of e^+ scattering angles (rad)				
	$\theta_{e^+} < .1$	$.1 < \theta_{e^+} < .2$	$.2 < \theta_{e^+} < .3$	$.3 < \theta_{e^+} < .4$	$.4 < \theta_{e^+} < .5$
$\sigma(\alpha(0))$ (pb)	222	22	13.2	10.0	8.3
N , (in 10^6)	111	11	6.6	5.0	4.1
$\langle Q^2 \rangle$ (GeV^2)	0.005	0.15	0.44	0.89	1.51
$1 - \frac{\sigma(t)}{\sigma(s+t)}$, (in 10^{-4})	0.6	52	130	255	415
$\langle \Delta\alpha_l \rangle$, (in 10^{-4})	34	99	115	125	133
$\langle \Delta\alpha_{\text{had}} \rangle$, (in 10^{-4})	0.4	11	23	35	44
$\frac{\sigma(\alpha(Q^2))}{\sigma(\alpha(0))} - 1$, (in 10^{-4})	69	223	281	327	365
$1/\sqrt{N}$, (in 10^{-4})	1.0	3.0	3.9	4.5	4.9

acceptance that is expected to be relatively free of background. The scattered electron and photon are required to be within the angular acceptance of the calorimeter ($20^\circ < \theta < 135^\circ$). The energies of the photon and wide-angle electron are required to be at least 2 GeV and the invariant mass of the pair is to be between 2 and 8 GeV. The angles and energies of particles referred to in this section are given in the BaBar laboratory frame.

The BaBar detector does not include an electron tagger for low backward angles, but it is envisaged that a detector could be put in place to tag electrons scattered above 300 mrad away from the $-z$ axis [14]. For the purposes of this study, however, events are classified into 100 mrad bins of positron scattering angles between 0 and 500 mrad. The Belle detector at the KEKB collider has an electron tagger for scattering in the angular range of 150 to 300 mrad in the backward direction [15].

The TEEGG event generator [13] is used to calculate the cross sections of events in the acceptances define above, and the results are summarized in Table 2. The calculations are done in lowest order, including the s and t channel processes but without vacuum polarization effects.

Some characteristics of the events inside the full acceptance, $\theta_{e^+} < 0.5$ rad, are shown in Fig. 4. The bulk of events are well away from the edges of most of the acceptance criteria, apart from the requirement on the minimum scattering angle of

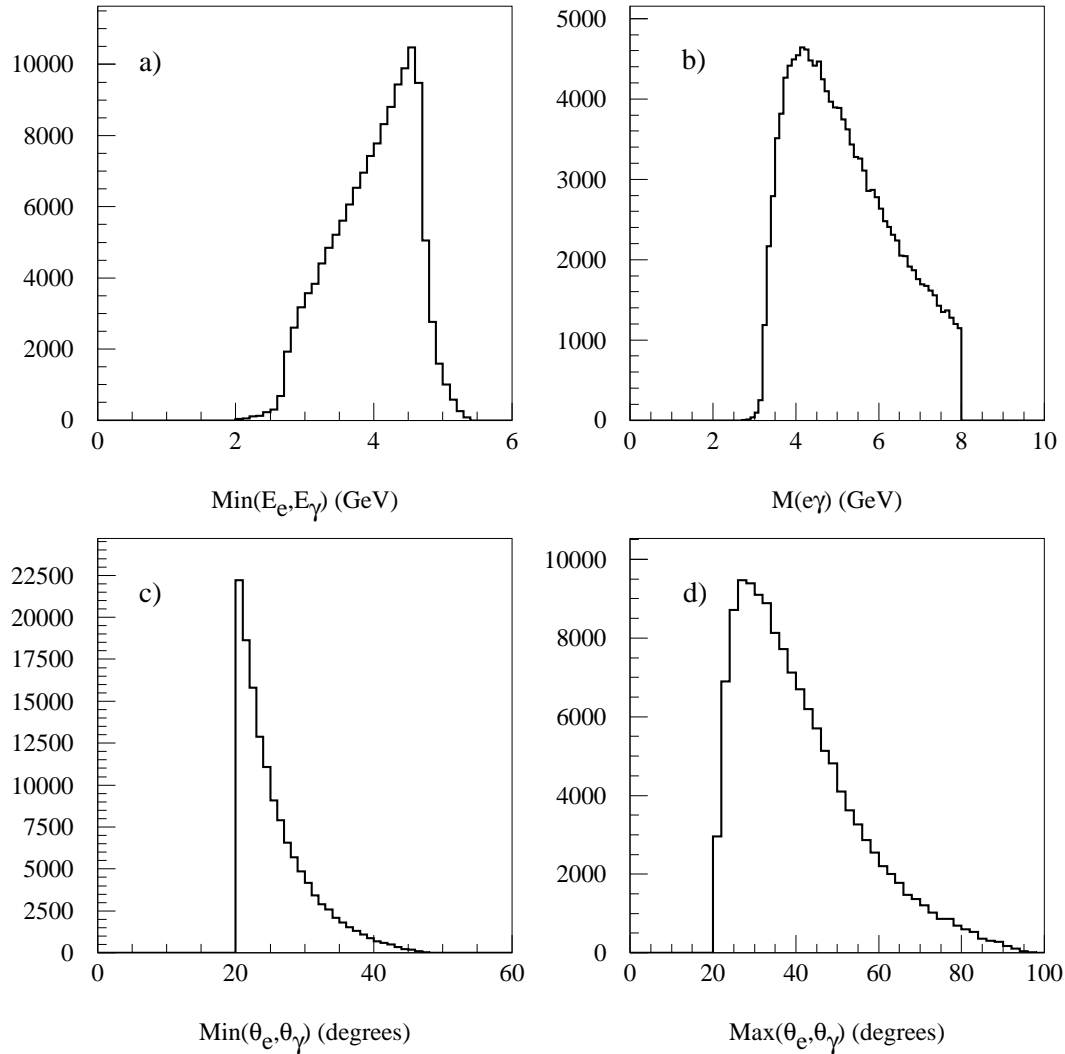


Fig. 4. Some distributions of TCRB scattering events in the BaBar acceptance for $\theta_{e^+} < 0.5$ rad. a) The minimum energy of the photon and wide angle electron (required to be above 2 GeV). The natural cutoff above about 2.5 GeV is due to momentum conservation in the 3 body final state. b) The $e\gamma$ invariant mass. This is required to be above 2 GeV, in order to reduce background from various processes, and below 8 GeV to reduce contamination from $2 \rightarrow 2$ processes, which would appear at the center-of-mass energy. c) The minimum scattering angle of the photon and wide angle electron (required to be above 20°). d) The maximum scattering angle of the photon and wide angle electron (required to be below 135°).

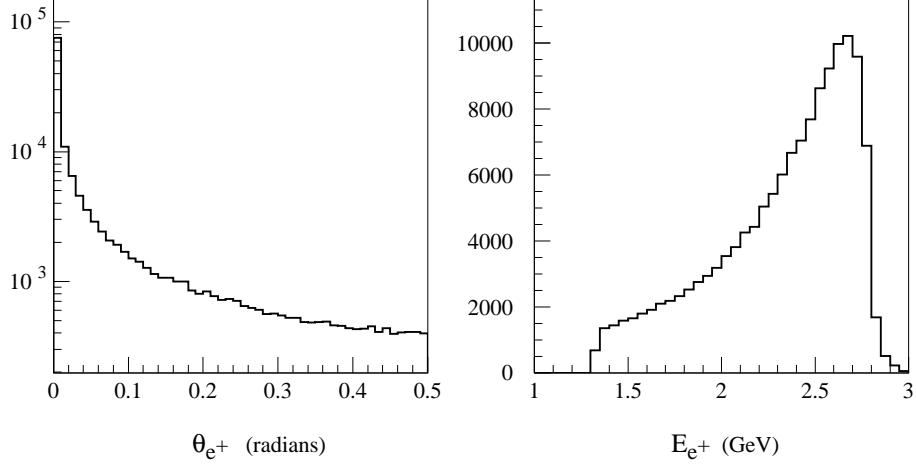


Fig. 5. Distributions of the low angle scattered positron. a) The scattering angle with respect to the $-z$ axis. b) The energy of the positron.

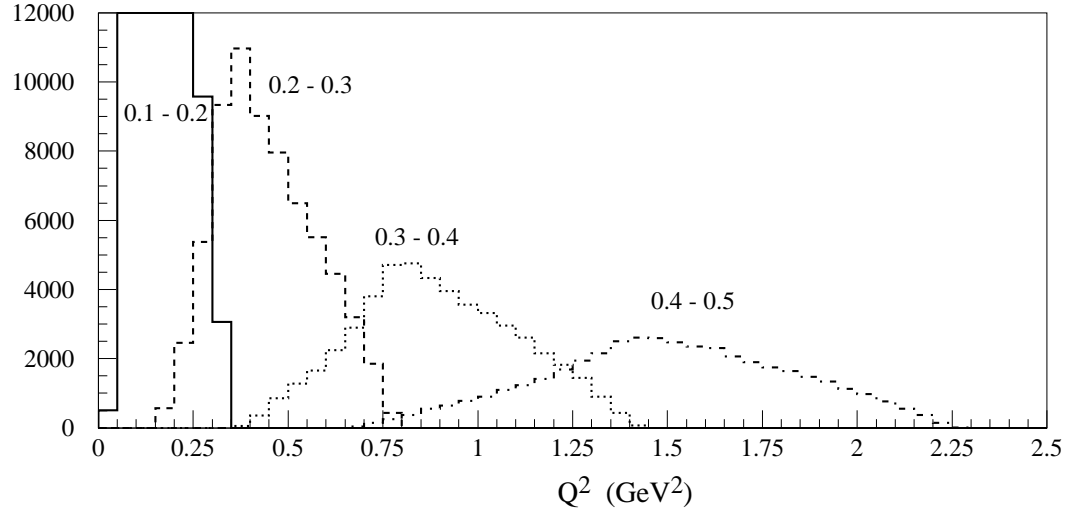


Fig. 6. The distributions of Q^2 are shown for the different bins in scattering angle of the low angle positron. The solid histogram is $0.1 < \theta_{e^+} < 0.2$; the dashed is $0.2 < \theta_{e^+} < 0.3$, the dotted is $0.3 < \theta_{e^+} < 0.4$, and the dot-dashed is $0.4 < \theta_{e^+} < 0.5$ (all in radians).

the electron and photon. Distributions of the low angle positron are shown in Fig. 5.

Vacuum polarization has different strength in the different bins of positron scattering angle due to the fact that the bins involve different values of Q^2 . Since the TCRB scattering process is dominated by the t channel contribution, the modification to the cross section due to vacuum polarization can be approximated by,

$$\sigma(\alpha(Q^2)) = \frac{\alpha^2(Q^2)}{\alpha^2(0)} \sigma(\alpha(0)). \quad (3)$$

Table 3

Summary of systematic uncertainties in the measurement of event ratios. The first row indicates the deviation in the double ratio from 1, due to vacuum polarization. The second row indicates the statistical uncertainty in the double ratios for each bin. The next rows show the deviations in the double ratio D_i for each bin for a number of situations that can result in systematic uncertainties. Note that the systematic uncertainties are correlated.

	Range of e^+ scattering angles (rad)			
	$.1 < \theta_{e^+} < .2$	$.2 < \theta_{e^+} < .3$	$.3 < \theta_{e^+} < .4$	$.4 < \theta_{e^+} < .5$
ΔD_i [vac. pol.] (in 10^{-4})	154	211	257	294
Statistical uncertainty (in 10^{-4})	3	4	5	5
ΔD_i [$\min(\theta_e, \theta_\gamma) > 20.2^\circ$] (in 10^{-4})	10	7	7	9
ΔD_i [$\min(E_e, E_\gamma) > 2.04$ GeV] (in 10^{-4})	0	0	1	27
ΔD_i [$M_{e\gamma}^2 < 62$ GeV 2] (in 10^{-4})	12	15	3	1
ΔD_i [$\Delta\theta_{e^+} = 1$ mrad] (in 10^{-4})	77	57	26	30
ΔD_i [radiative corrections] (in 10^{-4})	65	23	100	142

In order to measure the variation of $\alpha(Q^2)$ in a simple fashion, the ratio of event counts in each bin to that in the lowest angle bin can be used. In this way systematic uncertainties arising from detector acceptance can be reduced. Figure 6 shows the Q^2 distributions for the four samples above 100 mrad.

The event ratios, $R_i = \sigma(\theta_{\text{low},i} < \theta_{e^+} < \theta_{\text{high},i}) / \sigma(\theta_{e^+} < 0.1)$, can be measured and compared to the expected ratios in absence of vacuum polarization effects, $R_i(\alpha(0))$. Deviations in the double ratios, $\Delta D_i = R_i / R_i(\alpha(0)) - 1$, measure the strength of vacuum polarization. From the last row in Table 2 one can see that the the relative statistical precision of the event rates is $3 - 5 \times 10^{-4}$, which corresponds to relative statistical uncertainties in $\alpha(Q^2)$ of about 2×10^{-4} . This is still about twice as large as the present relative uncertainty in the prediction of $\alpha(Q^2)$, for Q^2 near 1 GeV 2 .

4 Systematic uncertainties

The statistical precisions of the event ratios are at the level of a few parts in 10^4 . It is a significant challenge to limit systematic effects in the measurement of event ratios to the same level. In this section, some of these effects are considered and are summarized in Table 3.

Calorimeter angular acceptance

Figure 4c shows that the events are very forward peaked. The number of accepted events is therefore very sensitive to the location of the cut on the minimum scatter-

ing angle. The shape of this distribution depends somewhat on Q^2 , so that the double ratios have a residual dependence on the precise location of the cut. For example, if the cut is moved to 20.2° , the double ratio changes by a factor of (10×10^{-4}) . The values are shown for each bin in Table 3.

Energy scale of the calorimeter

Modifying the minimum energy cut from 2 GeV to 2.04 GeV, results in a change in the double ratio of events for the larger Q^2 bins. Changing the maximum invariant mass from 8 to 7.9 GeV affects the double ratio most significantly for lower Q^2 bins.

Low angle tagger acceptance

As expected, the measurement requires a precise knowledge of the angular acceptance of the small angle scattered positrons. Table 3 shows the change in the double ratio that results in a change in all angular bins by 1 mrad. If the edges of the angular acceptance can be known to a precision of 0.1 mrad, the systematic error will be about the same magnitude as the statistical error. Additional corrections due the beam spot size and position in the interaction region and due to the beam divergence will have to be taken into account. They are generally well known on average, from the knowledge of the machine optics and monitoring of beam sizes and positions, such that the contribution to the systematic uncertainty will be small.

Radiative corrections

The TEEGG program implements photonic radiative corrections to the process of TCRB scattering using the equivalent photon approximation. The effect of these radiative corrections modifies the double ratio by significant amounts. The magnitude of the radiative correction needs to be known at the level of 10% or better, for this not to lead to a dominant systematic uncertainty. A better understanding of the sensitivity of radiative corrections requires a simulation of the experiment and perhaps a more exact calculation.

Background processes

Background events are expected to come from Bhabha scattering (when one electron undergoes bremsstrahlung in the detector material) and two photon final states

(when one photon converts). These backgrounds are reduced by the cut on the invariant mass. When these events are accompanied by initial state radiation, the invariant mass cut is no longer effective. Such events however do not exhibit the strong charge asymmetry of the wide-angle scattered electron, and thus the size of the remaining background can be measured directly in the data sample.

Another background source will be due to off-momentum particles lost from the beam. As off-momentum particles originate in beam-gas scattering, good vacuum conditions in the straight sections around the experiment will be important. The background rates due to off-momentum background particles reaching the detectors can be monitored by analyzing random beam crossing samples. This source of background can be distinguished from the signal through the use of kinematic constraints imposed by four-momentum conservation.

5 Measurement of TCRB scattering at LEP

The integrated luminosity recorded at LEP is three orders of magnitude less than that expected for PEP II. In addition, the cross section for TCRB scattering is lower for a fixed acceptance at higher energies. Nevertheless, it is possible to make an interesting measurement using the LEP data set.

The cross section for TCRB scattering at LEP energies for configurations where both the electron and photon are scattered into the central detector is small, typically a few pb. By requiring instead that the photon scatters into the forward detector (used for precision luminosity measurements of Bhabha scattering), the cross section increases by more than a factor of 30.

The set of requirements considered for LEP1 and LEP2 are summarized below. The electron is required to be scattered in the forward hemisphere ($0 < \cos \theta < 0.9$) and a forward detector tag (due to the photon with $25 < \theta_\gamma < 58$ mrad) is required in the same hemisphere. The minimum transverse momentum of the wide angle scattered electron is set to 1.1 GeV for LEP1 and 2.4 GeV at LEP2. The minimum energy of the tagging photon is 30 (70) GeV for LEP1 (LEP2).

The TEEGG generator is used to evaluate the cross sections in these acceptances. Tables 4 and 5 summarize the measurements at LEP1 and LEP2, assuming integrated luminosities of 100 and 400 pb⁻¹, respectively. In the lower two rows of the last column of these tables, it is seen that the running of the fine structure constant modifies the cross section by about twice the statistical uncertainty for both cases.

Some characteristics of the events are shown in Figs. 7 and 8. Systematic uncertainties will be smaller than the statistical uncertainties provided the photon angular acceptance is known with 0.1 mrad, and the scale of the transverse momentum of

Table 4

Summary of calculations for TCRB scattering for the LEP acceptances. See the caption for Table 2 for an explanation of the entries.

	Range of e^+ scattering angles (mrad)				
	$\theta_{e^+} < 25$	$25 < \theta_{e^+} < 36$	$36 < \theta_{e^+} < 47$	$47 < \theta_{e^+} < 58$	$25 < \theta_{e^+} < 58$
$\sigma(\alpha(0))$ (pb)	486	96	66	55	217
N , (in 10^3)	49	9.6	6.6	5.5	22
$\langle Q^2 \rangle$ (GeV) ²	0.042	1.91	3.59	5.77	3.40
$1 - \frac{\sigma(t)}{\sigma(s+t)}$, (in 10^{-2})	0.004	0.36	0.63	0.89	0.58
$\langle \Delta\alpha_l \rangle$, (in 10^{-2})	0.30	1.37	1.48	1.56	1.45
$\langle \Delta\alpha_{\text{had}} \rangle$, (in 10^{-2})	0.02	0.49	0.62	0.73	0.60
$\frac{\sigma(\alpha(Q^2))}{\sigma(\alpha(0))} - 1$, (in 10^{-2})	0.7	3.8	4.3	4.8	4.2
$1/\sqrt{N}$, (in 10^{-2})	0.5	3.2	3.9	4.3	2.1

Table 5

Summary of calculations for TCRB scattering for the LEP2 acceptances. See the caption for Table 2 for an explanation of the entries.

	Range of e^+ scattering angles (mrad)				
	$\theta_{e^+} < 25$	$25 < \theta_{e^+} < 36$	$36 < \theta_{e^+} < 47$	$47 < \theta_{e^+} < 58$	$25 < \theta_{e^+} < 58$
$\sigma(\alpha(0))$ (pb)	110	20.1	14.0	11.6	46
N , (in 10^3)	44	8.0	5.6	4.6	18
$\langle Q^2 \rangle$ (GeV) ²	0.19	9.0	16.9	27.2	16.1
$1 - \frac{\sigma(t)}{\sigma(s+t)}$, (in 10^{-2})	0.004	0.36	0.63	0.89	0.58
$\langle \Delta\alpha_l \rangle$, (in 10^{-2})	0.37	1.64	1.76	1.85	1.73
$\langle \Delta\alpha_{\text{had}} \rangle$, (in 10^{-2})	0.05	0.84	1.00	1.12	0.96
$\frac{\sigma(\alpha(Q^2))}{\sigma(\alpha(0))} - 1$, (in 10^{-2})	0.8	5.1	5.7	6.2	5.6
$1/\sqrt{N}$, (in 10^{-2})	0.5	3.5	4.2	4.7	2.3

the wide scattered electron is known within 50 and 100 MeV for LEP1 and LEP2 respectively.

6 Summary

A precise measurement of vacuum polarization for $Q^2 < 1.5 \text{ GeV}^2$ could be possible at the asymmetric B factory, PEP-II (with an improvement in precision by an order of magnitude compared to previous measurements). A plot of the running of the fine structure constant that could result from such a measurement is shown in Fig. 9. While the relative statistical precision of approximately 2×10^{-4} is somewhat larger than the present uncertainties in the calculations of $\alpha(Q^2)$, such a measurement could still give an impressive illustration of the running of one of the most fundamental constants in nature.

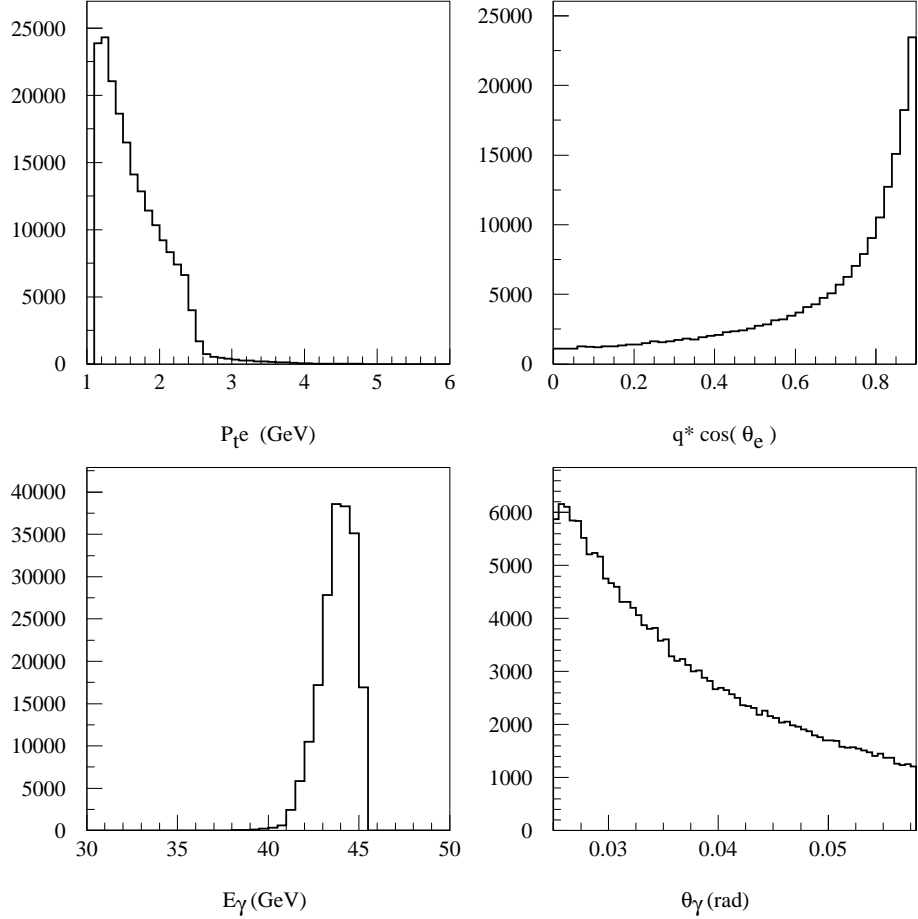


Fig. 7. Distribution for the LEP1 acceptance.

With the data sample recorded at LEP it is possible to use this approach to confirm, at the few standard deviations level, that the fine structure constant runs in the range $\sqrt{-t}$ from near 0 to 5 GeV.

It may be possible to apply the technique proposed here at the KEKB collider or at other high luminosity electron positron colliders. In addition, approaches that have already been applied at Tristan and LEP, using Bhabha scattering and muon pair production, can be applied at the high luminosity colliders to further improve the precision on the determination of vacuum polarization, and to extend the range in Q^2 .

The authours would like to thank W. Kozanecki for useful discussions.

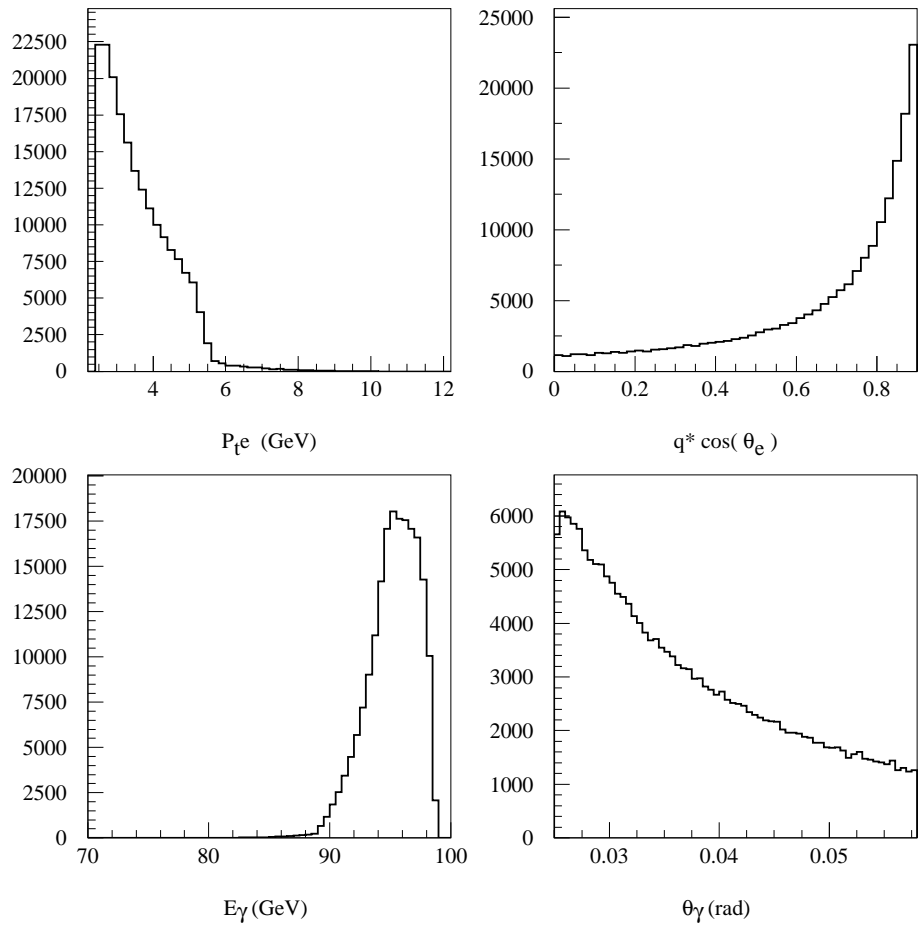


Fig. 8. Distribution for the LEP2 acceptance.

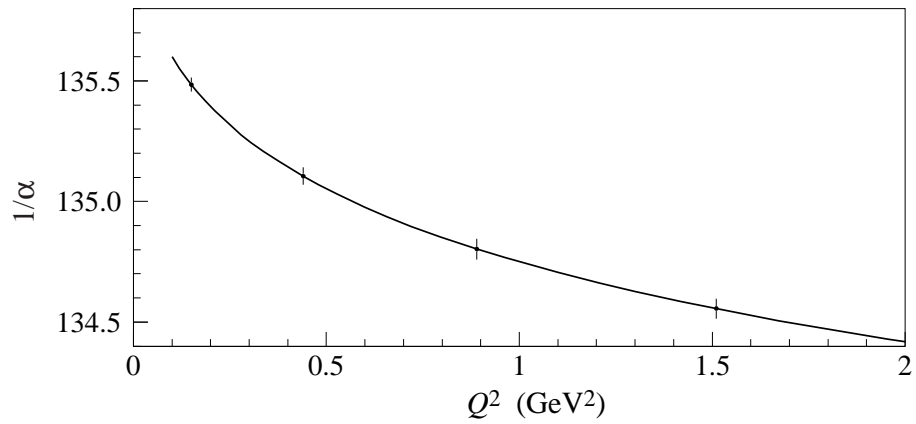


Fig. 9. The potential measurement of the running of α at PEP-II. The error bars are statistical only.

References

- [1] LEP Electroweak Working Group. <http://lepewwg.web.cern.ch/LEPEWWG/>.
- [2] **Muon g-2** Collaboration, H. N. Brown *et al.*, “Precise measurement of the positive muon anomalous magnetic moment,” *Phys. Rev. Lett.* **86** (2001) 2227–2231, [hep-ex/0102017](https://arxiv.org/abs/hep-ex/0102017).
- [3] A. Czarnecki and W. J. Marciano, “The muon anomalous magnetic moment: Standard model theory and beyond,” [hep-ph/0010194](https://arxiv.org/abs/hep-ph/0010194).
- [4] A. Czarnecki and W. J. Marciano, “The muon anomalous magnetic moment: A harbinger for ‘new physics,’” [hep-ph/0102122](https://arxiv.org/abs/hep-ph/0102122).
- [5] M. Steinhauser, “Leptonic contribution to the effective electrodynamical coupling constant up to three loops,” *Phys. Lett.* **B429** (1998) 158–161.
- [6] H. Burkhardt and B. Pietrzyk, “Update of the hadronic contribution to the QED vacuum polarization,” LAPP-EXP-2001-03, submitted to *Phys. Lett. B*.
- [7] J.E. Augustin *et al.*, “Evidence for the ϕ -Meson Contribution to Vacuum Polarization Obtained with the Orsay e^+e^- Colliding-Beam Ring,” *Phys. Rev. Lett.* **30** (1972) 462–465.
- [8] **TOPAZ** Collaboration, I. Levine *et al.*, “Measurement of the electromagnetic coupling at large momentum transfer,” *Phys. Rev. Lett.* **78** (1997) 424–427.
- [9] **VENUS** Collaboration, S. Odaka *et al.*, “Measurement of the running of effective QED coupling at large momentum transfer in the space-like region,” *Phys. Rev. Lett.* **81** (1998) 2428.
- [10] **L3** Collaboration, M. Acciarri *et al.*, “Measurement of the running of the fine-structure constant,” *Phys. Lett.* **B476** (2000) 40–48, [hep-ex/0002035](https://arxiv.org/abs/hep-ex/0002035).
- [11] D. Karlen, “A study of low Q^2 radiative Bhabha scattering,” SLAC-0325, (PhD. thesis).
- [12] D. Karlen *et al.*, “Measurement of single and double radiative low Q^2 Bhabha scattering at $E(\text{cm}) = 29\text{-GeV}$,” *Phys. Rev.* **D39** (1989) 1861.
- [13] D. Karlen, “Radiative Bhabha scattering for singly tagged and untagged configurations,” *Nucl. Phys.* **B289** (1987) 23.
- [14] D. Boutigny *et al.*, “BABAR Technical Design Report.” SLAC-R-95-457, 1995.
- [15] S.Mori (Ed.), “The Belle Detector.” KEK Progress Report 2000-4, submitted to NIM.